Applied Surface Science 284 (2013) 514–522

Contents lists available at ScienceDirect

Applied Surface Science

journal homepage: www.elsevier.com/locate/apsusc

Adsorption of silver on glucose studied with MIES, UPS, XPS and AFM

S. Dahle[a,b], J. Meuthen[a], W. Viöl[b,c], W. Maus-Friedrichs[a,d,*]

[a] Institut für Physik und Physikalische Technologien, Technische Universität Clausthal, Leibnizstrasse 4, 38678 Clausthal-Zellerfeld, Germany
[b] Hochschule für Angewandte Wissenschaft und Kunst, Fakultät für Naturwissenschaften und Technik, Von-Ossietzky-Straße 99, 37085 Göttingen, Germany
[c] Anwendungszentrum für Plasma und Photonic APP, Fraunhofer-Institut für Schicht- und Oberflächentechnik IST, Von-Ossietzky-Straße 99, 37085 Göttingen, Germany
[d] Clausthaler Zentrum für Materialtechnik, Technische Universität Clausthal, Leibnizstrasse 4, 38678 Clausthal-Zellerfeld, Germany

ARTICLE INFO

Article history:
Received 13 December 2012
Received in revised form 23 July 2013
Accepted 24 July 2013
Available online 3 August 2013

PACS:
68.37.Ps
81.15.Dj
82.45.Mp
82.80.Pv

Keywords:
Silver
Glucose
Valence band
Metastable induced electron spectroscopy
Ultraviolet photoelectron spectroscopy
X-ray photoelectron spectroscopy
Atomic force microscopy
Reduction

ABSTRACT

The adsorption behavior of silver atoms on a glucose film and their interaction was investigated by metastable induced electron spectroscopy (MIES), ultraviolet photoelectron spectroscopy (UPS) and X-ray photoelectron spectroscopy as well as atomic force microscopy. Glucose is found to form micro droplets on gold substrates with typical diameters/dimensions of about 400 nm. The discussion of the valence band structures is carried out in comparison to various model systems. The adsorbed silver atoms on top of the glucose have been found to form silver nanoparticles that get encapsulated by a large film of glucose. Furthermore, the reduction of the glucose in the presence of these silver particles is observed. This effect is discussed with the most probable origin of the reduction being the charging by electron spectroscopy.

1. Introduction

The adsorption of silver on different organic substrates is of great technological interest for various applications, such as corrosion protection, RF shielding, reflective coatings, and many more. Over the past 20 years, especially silver nanoparticle coatings drastically increased in importance, due to their outstanding functionality. For instance, silver nanoparticles are known to enhance the efficiency of organic light emitting devices [1], whereas silver films on TiO_2 nanoparticles enhance photocatalytic reaction rates [2,3]. One of the most common applications of silver particles is the functionalization of surfaces because of their antibacterial properties [4–7]. This may be useful especially on wood surfaces to preserve them from aging through attack of microorganisms by other means than lacquering or impregnation.

The relevance of surface modifications of wood by means of laser or plasma technology increased substantially in the past few years [8–20]. Low-temperature radio frequency plasma treatment is found to enhance the durability of nanoparticle coatings [5]. Therefore, a combined method of plasma-treatment and metal nanoparticle coating may be quite interesting for industrial applications regarding economical aspects as well as an improvement of functionality. The combination of both surface treatments is possible in numerous ways, e.g. by using a plasma-jet with precursor gases [21,22]. To understand the interactions with wood surfaces, several model systems are used to resemble the organic groups of lignin and cellulose. For cellulose these are the molecular precursors cellobiose and glucose. The effect of plasma treatments on these molecules was studied previously [23,24]. In the course of that work a significant decrease of carbon–oxygen single bonds was observed subsequent to plasma treatments in argon. Along with the accumulation of carbon which is not bound to oxygen this indicates a reduction of the molecules at the surface. The fraction of carbon=oxygen double bonds almost does not change [23].

In this study, first results of the adsorption behavior of silver on glucose films of different thicknesses are presented. These results are part of a research project concerning the interaction of metals (Ag, Ti) with wood surfaces particularly with regard to a

* Corresponding author. Tel.: +49 5323722310; fax: +49 5323723600.
E-mail address: w.maus-friedrichs@pe.tu-clausthal.de (W. Maus-Friedrichs).

0169-4332/$ – see front matter © 2013 Elsevier B.V. All rights reserved.
http://dx.doi.org/10.1016/j.apsusc.2013.07.126

preliminary plasma treatment. Glucose serves as one main precursor that is expected to yield important results to improve the understanding of such complex systems as wood. The final aim is to render a combined functionalization by plasma treatment and metal coating in one process step.

The interaction of silver and glucose has been employed to prepare silver nanoparticles [7,25–31], where glucose acts as reducing agent or in some cases as surface active agent, when bonded to siloxane. During the interaction of glucose and silver, a localized surface plasmon resonance gives rise to the use of silver as biosensor for glucose [32]. Furthermore, silver nanoparticles can be used as biosensor for glucose when coated with polyethyleneimine [33] or when glucose oxidase has been immobilized onto the surface from a solution of H_2O_2 and glucose [34–39]. Combining these sensors with luminol, the H_2O_2 side product from the sensoring reaction is inducing an electrogenerated chemiluminescence [40].

When applying voltage cycles between −0.2 V and 0.8 V, silver nanoparticles have been found to oxidize glucose catalytically [41]. Additionally, this oxidation behavior is used with bimetallic materials based on silver which exhibit great performances for microfluidic fuel cells for glucose [42,43].

The detailed interpretation of MIES or UPS spectra of glucose is rather difficult since the literature lacks of any reference for the valence band structures of glucose. Thus, we follow the ansatz of L. Klarhöfer, taking into account the valence states of different kinds of model systems [24] in the following way: The typical binding energy for valence bands of hydrocarbons, i.e. C 2p based molecular orbitals (MO) from CH_3 groups, as well as from carbon atoms inside organic chains at C—C or C=C bonds are deducted from the valence states of propane [44], propene [44], polypropylene [45,46], polyethylene [47] and benzene [44]. The C 2p and O 2p based molecular orbitals were identified by comparison with phenol [44] and polyvinyl alcohol (PVA) [48–50] for OH groups bound to organic molecules, polyoxyethylene (POE) [48] for C—O—C groups, and poly(methyl methacrylate) (PMMA) [51,52] for O—CH_3 groups. Polycarbonate (PC) [53] and PMMA have both been used as model systems for valence band states of C=O groups.

2. Experimental details

An ultra high vacuum apparatus with a base pressure of 5×10^{-11} hPa, which has been described in detail previously [54–57], is used to carry out the experiments. All measurements were performed at room temperature.

Electron spectroscopy is performed using a hemispherical analyzer (Leybold EA 10) in combination with a source for metastable helium atoms (mainly $He^* {}^3S_1$) and ultraviolet photons (HeI line). A commercial non-monochromatic X-ray source (Fisons XR3E2-324) is utilized for XPS.

During XPS, X-ray photons hit the surface under an angle of 80° to the surface normal, illuminating a spot of several mm in diameter. For all measurements presented here, the Al K_α line with a photon energy of 1486.6 eV is used. Electrons are recorded by the hemispherical analyzer with an energy resolution of 1.1 eV for detail spectra and 2.2 eV for survey spectra, respectively, under an angle of 10° to the surface normal. All XPS spectra are displayed as a function of binding energy with respect to the Fermi level.

For quantitative XPS analysis, photoelectron peak areas are calculated via mathematical fitting with Gauss-type profiles using OriginPro 7G including the PFM fitting module, which applies Levenberg–Marquardt algorithms to achieve the best agreement between experimental data and fit. To optimize our fitting procedure, Voigt-profiles have been applied to various oxidic and metallic systems but for most systems the Lorentzian contribution converges to 0. Therefore all XPS peaks are fitted with Gaussian shapes. Photoelectric cross sections as calculated by Scofield [58] with asymmetry factors following [59,60] and inelastic mean free paths from the NIST database [61] (using the database of Tanuma, Powell and Penn for elementary contributions and the TPP-2M equation for molecules) as well as the energy dependent transmission function of our hemispherical analyzer are taken into account when calculating the stoichiometries. According to Ref. [23], the detail spectra of the C 1s region are analyzed by fitting single Gaussians of equal width for every chemical species. It is assumed to be composed of contributions from carbon—carbon or carbon—hydrogen bonds (C_0), carbon—oxygen bonds (C_1), carbon linked to two oxygen atoms or twice to one oxygen atom (C_2), and a shake-up feature (C^*). For neither of the spectra any contributions of carboxyl groups were found. During the fitting procedure, the relative positions i.e. binding energy differences have been fixed to 1.5 eV for C_0—C_1, 2.9 eV for C_0—C_2 and 6.5 eV for C_0—C^*.

MIES and UPS are performed applying a cold cathode gas discharge via a two-stage pumping system. A time-of-flight technique is employed to separate electrons emitted by He^* (MIES) from those caused by HeI (UPS) interaction with the surface. The combined He^*/HeI beam strikes the sample surface under an angle of 45° to the surface normal and illuminates a spot of approximately 2 mm in diameter. The spectra are recorded simultaneously by the hemispherical analyzer with an energy resolution of 220 meV under normal emission within 140 s.

MIES is an extremely surface sensitive technique probing solely the outermost layer of the sample, because the He^* atoms interact with the surface typically 0.3 to 0.5 nm in front of it. This may occur via a number of different mechanisms depending on surface electronic structure and work function, as is described in detail elsewhere [62–64]. Only the processes relevant for the spectra presented here shall be discussed shortly.

During Auger Deexcitation (AD), an electron from the sample fills the 1s orbital of the impinging He^*. Simultaneously, the He 2s electron carrying the excess energy is emitted. The resulting spectra reflect the Surface Density of States (SDOS) directly. AD-MIES and UPS can be compared and allow a distinction between surface and bulk effects. AD takes place for all systems shown here.

On pure and partly oxidized metal surfaces with a work function beyond about 3.5 eV, Auger neutralization (AN) occurs as long as the surface shows metallic behavior. As a result the impinging He^* atom is ionized in the vicinity of the surface by resonant transfer (RT) of its 2s electron in unoccupied metallic surface states. Afterwards, the remaining He^+ ion is neutralized by a surface electron thus emitting a second surface electron carrying the excess energy. The observed electron spectrum is rather structureless and originates from a self convolution of the surface density of states (SDOS).

All MIES and UPS spectra are displayed as a function of the electron binding energy with respect to the Fermi level, thus being able to compare MIES and UPS spectra more easily. Obviously, the binding energy scale is only valid for the AD process. Nevertheless, all spectra including structures originating in the AN process have also been displayed in this particular manner. The surface work function can be determined from the high binding energy onset of the MIES or the UPS spectra with an accuracy of ±0.1 eV.

Atomic force microscopy (AFM) is applied to study the surface topography and determine the size of the silver nanoparticles. A Veeco Dimension 3100 SPM is employed to perform the AFM measurements in Tapping Mode. Silicon cantilevers (NSC15 with Al backside coating from Mikromasch) with a resonance frequency of about 308 kHz and a spring constant of about 40 N/m were used together with an optical lever detection technique. All images were gained with a line-scan frequency of 0.5 Hz or 1 Hz, respectively, with 512 pixels for each of the 512 lines.

The experiments on glucose were carried out on inert Au substrates with (1 1 1) or (1 0 0) crystal surfaces. These substrates have

been cleaned prior to the experiments by Ar-sputtering at 3 kV and 5 mA for 60 min and subsequent heating up to 1000 K. The Ag reference was prepared by adsorption onto a Si(1 0 0) substrate, which was preliminary cleaned by flashing up to 1400 K.

Silver (Sigma–Aldrich, 99%) was evaporated with a commercial UHV evaporator (Omicron EFM3) onto the samples. On a clean Si(1 0 0) target metallic silver films grow at a rate of 0.23 nm min^{-1} at room temperature when evaporated with an Ag^+ ion flux of 1 μA at the fluxmeter of the EFM3. This flux is a degree for the number of Ag atoms moving toward the sample per second. The film growth rate for Ag has been estimated from the Si 2p peak attenuation in XPS.

D-(+)-Glucose (Sigma–Aldrich Co., >99.5%) was evaporated in a directly connected preparation chamber (base pressure < 10^{-9} hPa) using a temperature controlled evaporator (Kentax TCE-BS). During all experiments glucose has been evaporated at 140 °C.

3. Results and discussion

In this section, we present our results for the adsorption of silver on glucose that was preliminary evaporated onto an Au(1 1 1) surface. Glucose films have been prepared as described in Section 2 at thicknesses of about 7.1 nm after 60 s of evaporation for the thick film and 1.1 nm after 24 s of evaporation for the thin film. Film thicknesses were calculated from the attenuation of the Au $4f_{7/2}$ peak in XPS by the adsorbates [64]. For better comprehensibility, results and discussions are divided into two parts, the spectroscopic and the microscopic results.

3.1. Spectroscopic results

Fig. 1 shows MIES (left) and UPS HeI (top right) spectra of a thick film of glucose on Au(1 1 1) as prepared (black lines, "A"), after silver adsorption (red lines, "B") and after subsequent exposure to 3.8×10^{13} L of air (blue lines, "C"), as well as a thin film of glucose on Au(1 0 0) after silver adsorption (orange lines, "D") and a thick film of pure silver on a cleaned Si(1 0 0) waver (green lines, "E"), as well as UPS HeII spectra (bottom right) of the thick film of glucose before (black lines, "A") and after silver adsorption (red lines, "B"). (For interpretation of the references to color in the text, the reader is referred to the web version of the article.)

The MIES spectrum of pure glucose ("A") consists of three main features around 6.1 eV, 9.9 eV and between 11.9–13.4 eV. An additional shoulder is visible around 7.8 eV, while structures are too broad in UPS to be distinguished clearly. The feature at 6.1 eV is related to π-type MO from C—H bonds like the C 4a" state of phenol at 8.7 eV [44]. The slightly lower binding energy for glucose compared to the phenol is most likely be due to the inhibiting impact of the multiple OH groups on the π system of the carbon ring. Even though the hybridization of the π orbitals from the C 2p and O 2p atomic orbitals at the OH groups attached to the carbon ring leads to a higher localization of the resulting molecular orbitals, the formation of a ringlike π system is possible. Nevertheless, the sharper localization of the hybridized MO out of the carbon ring plane clearly leads to a smaller overlap of the π orbitals and thus any π system formation can only yield significantly less gain of energy compared to benzene. Therefore, the binding energies of such a π ring must always be lower than the corresponding states of benzene. The same arguments as given above for the first glucose valence band state support the interpretation of the structure at 9.9 eV to be related to the phenol C 3a" MO at 9.39 eV [44] and thus to C—H bonds.

The slightly broadened structure between 11.9–13.4 eV consists of different types of bonds. Since any potential π system should be found at lower binding energies compared to benzene, it is quite unlikely to have a pronounced fraction of states related to such a π system within this broadened structure as corresponding to the benzene states C $1e_{1g}$ at 9.25 eV, C $3e_{2g}$ at 11.53 eV and C $1a_{2u}$ at 12.38 eV, or the phenol states C 2a" at 11.59 eV, C 21a' at 12.02 eV, C 20a' at 12.61 eV and C 19a' at 13.44 eV, respectively [44]. Thus, this broad band is due to the σ type oxygen state corresponding to C—O—H groups like the orbital found for polycarbonate from 12.9 eV to 13.8 eV [53]. The weak structure around 7.8 eV in MIES represents the OH groups' 1π state [65].

The MIES spectrum of a pure silver film (green line, "E") reveals two main structures between 2–6 eV and 6–11 eV belonging to the Auger neutralization (AN) process involving the Ag 4d and Ag 5s states [66]. The UPS HeI spectrum shows the Ag 4d structure around 5.5 eV as well as some intensity up to the Fermi level due to the conduction band [66].

The adsorption of silver on the thick film of glucose (see red MIES and UPS spectra, "B") does induce a broadening of the valence structures of glucose, while no features corresponding to silver can be observed, as compared to the silver reference spectra (green lines, "E"). This is best seen in the UPS HeI and HeII spectra for the absence of the Ag 4d structure which is usually appearing with comparatively high intensities. In the MIES spectrum the low energy AN structure with its maximum around 3.5 eV should be clearly visible as shoulder alongside the valence states of glucose. After the adsorption of silver, the thin film of glucose exhibits (orange lines, "D") a mixture of the Ag 4d and the Au 5d structures in UPS, while the typical AN features from the Ag 4d and Ag 5s states are still not visible in MIES. This indicates the presence of the silver beneath the glucose film, thus the silver atoms can interact with the UV photons while being out of reach for the metastable helium atoms. Some of the silver may be located at the interface between the gold substrate and the glucose film, while the appearance of the gold structures indicates a decreasing thickness of the glucose film. Nevertheless, the gold substrate is not visible in any of the MIES spectra, thus the silver found in the UPS spectrum for the thin film of glucose after silver adsorption must be located within the glucose film, just beneath the surface. For both thicknesses of the glucose film, the adsorption of silver leaves the peak at 6.1 eV almost unchanged in shape while its intensity gets slightly decreased.

The feature around 10 eV appears to be shifted slightly toward higher binding energies upon silver adsorption. This indicates an increased impact of oxygen states through the 3σ state of physisorbed water at 11.8 eV [65]. The exposure to air and thus the exposure to water, oxygen and others subsequent to the adsorption of silver on the thick film of glucose (blue lines, "C") leaves the features around 6 eV, 10 eV and above 12.5 eV unchanged. The oxygen state around 8 eV gets slightly increased, thus supporting the assumption of its correlation to physisorbed water. The MIES spectrum shows an apparent decrease of intensity around 11.6 eV that most probably is due to an interaction between the adsorbed water with the OH groups of the glucose.

Fig. 2 displays XPS spectra of the C 1s region of a thick film of glucose on Au(1 1 1) as prepared (black lines and squares; top spectrum), after silver adsorption (red lines and triangles; upper middle spectrum) and after subsequent exposure to 3.8×10^{13} L of air (blue lines and circles; lower middle spectrum), as well as a thin film of glucose on Au(1 0 0) after silver adsorption (orange lines and diamonds; bottom spectrum). (For interpretation of the references to color in the text, the reader is referred to the web version of the article.) The thick film of glucose yields five peaks with the main one corresponding to C—O bonds. The adjacent peak at the high binding energy side belongs to C=O bonds, while the one at the low binding energy side originates from aliphatic carbon atoms. The outermost, minor peaks most probably correspond to adventitious carbon and carbonate groups at the sample holder. The presence of carboxyl groups and aliphatic carbon as well as a slightly too large fraction

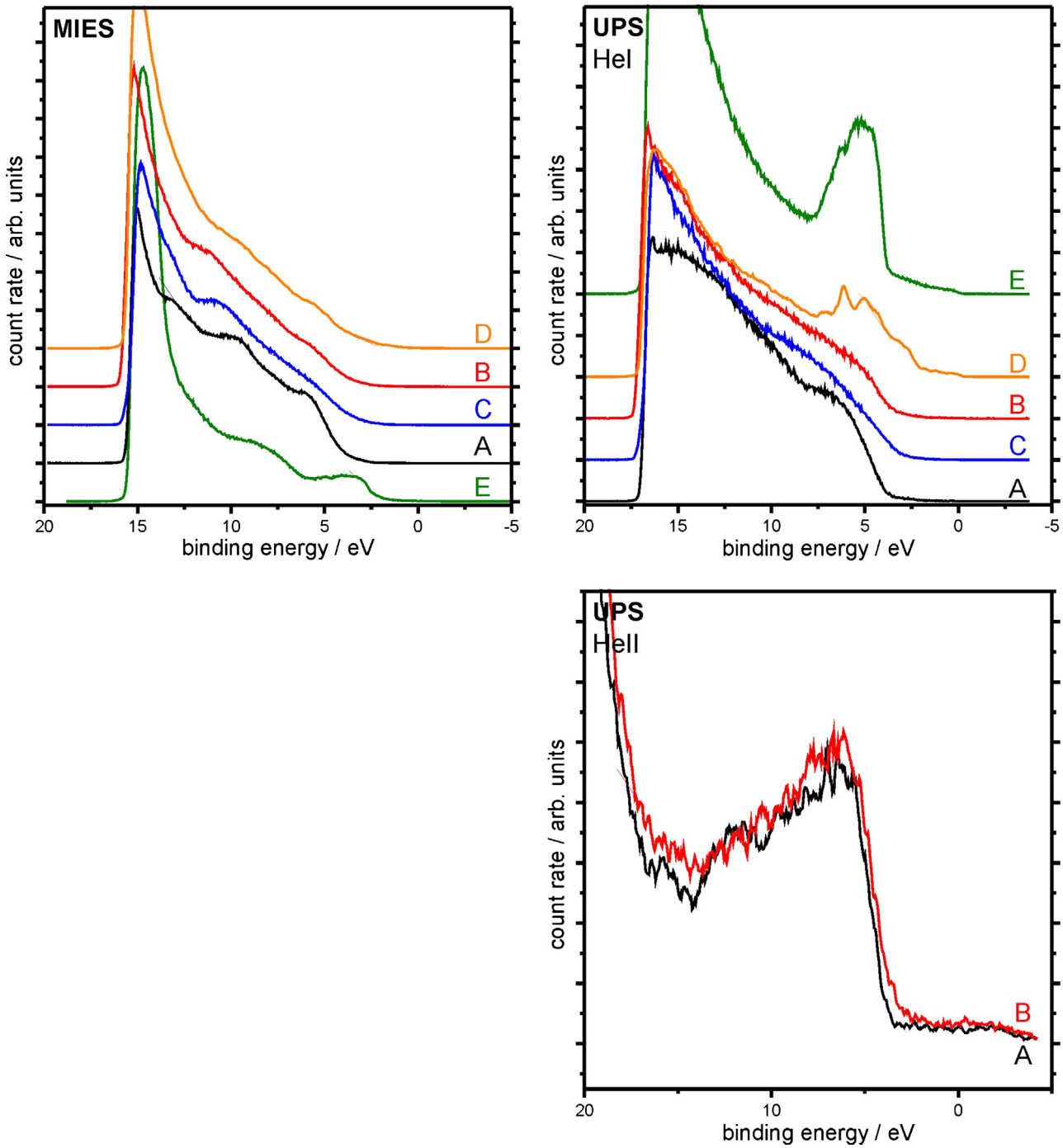

Fig. 1. MIES (left) and UPS HeI (top right) spectra of a thick film of glucose on Au(1 1 1) as prepared (black lines, "A"), after silver adsorption (red lines, "B") and after subsequent exposure to 3.8×10^{13} L of air (blue lines, "C"), as well as a thin film of glucose on Au(1 0 0) after silver adsorption (orange lines, "D") and a thick film of pure silver on a cleaned Si(1 0 0) waver (green lines, "E"), as well as UPS HeII spectra (bottom right) of the thick film of glucose before (black lines, "A") and after silver adsorption (red lines, "B").

of carbonyl groups compared to the methoxyl groups indicate the dissociation of some of the glucose molecules upon evaporation. During the further steps of the experiment, the two minor peaks as well as the carboxyl remain nearly unchanged. The methoxyl groups on the other hand get reduced to aliphatic carbon upon both, the silver adsorption as well as the exposure to water.

The silver coated, thin film of glucose exhibits a similar distribution of the aliphatic, methoxyl and carbonyl groups as found earlier for the thick film of pure glucose, while the overall intensity is seriously smaller in this case due to the smaller film thickness. Thus, the carbon peak attributed to adventitious carbon on the sample holder appears to be much more prominent. All XPS fit results for the C 1s regions have been summarized in detail in Table 1.

Fig. 3 contains XPS spectra of the O 1s region of a thick film of glucose on Au(1 1 1) as prepared (black lines and squares; top spectrum), after silver adsorption (red lines and triangles; upper middle spectrum) and after subsequent exposure to 3.8×10^{13} L of air (blue lines and circles; lower middle spectrum), as well as a thin film of glucose on Au(1 0 0) after silver adsorption (orange lines and diamonds; bottom spectrum). (For interpretation of the references to color in the text, the reader is referred to the web version of the article.) The thick film of glucose shows just one single peak, which

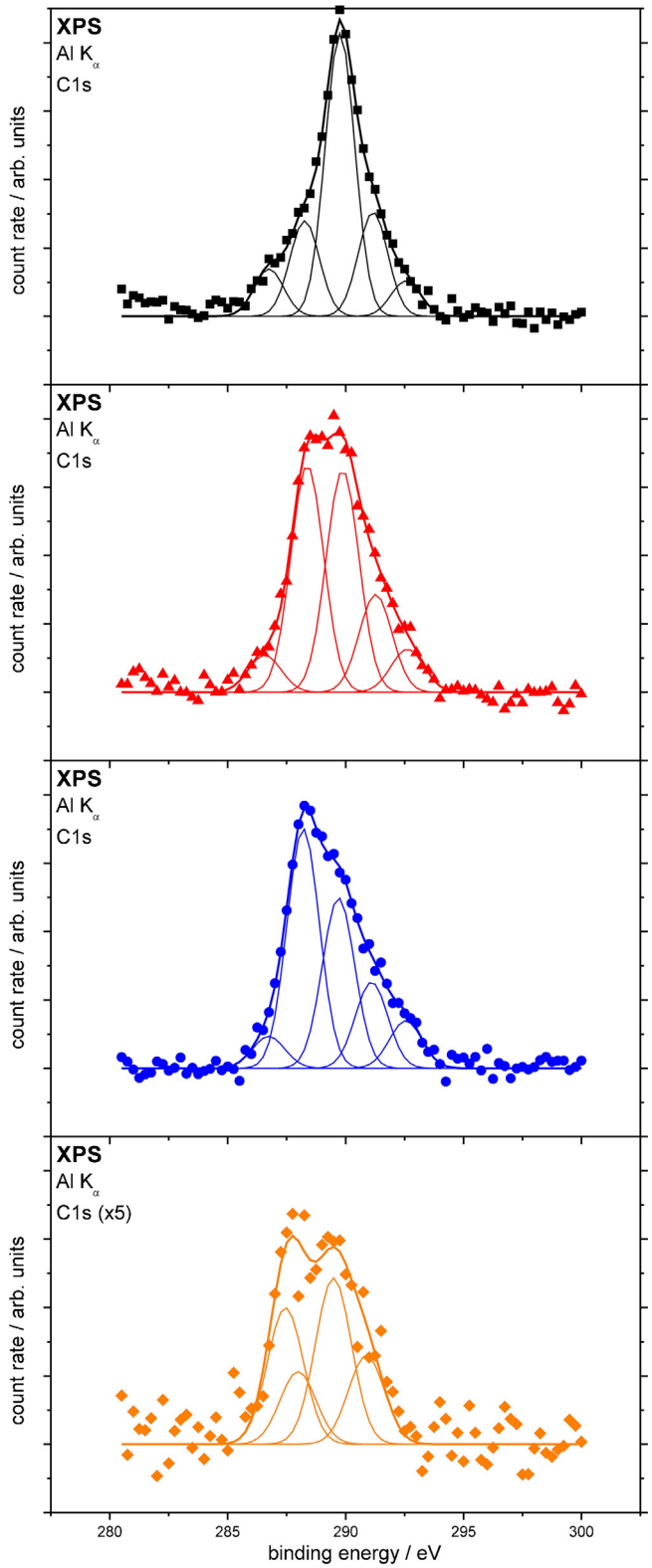

Fig. 2. XPS spectra of the C 1s region of (in order of appearance from top to bottom) a thick film of glucose on Au(1 1 1) as prepared (black lines and squares), after silver adsorption (red lines and triangles) and after subsequent exposure to 3.8×10^{13} L of air (blue lines and circles), as well as a thin film of glucose on Au(1 0 0) after silver adsorption (orange lines and diamonds).

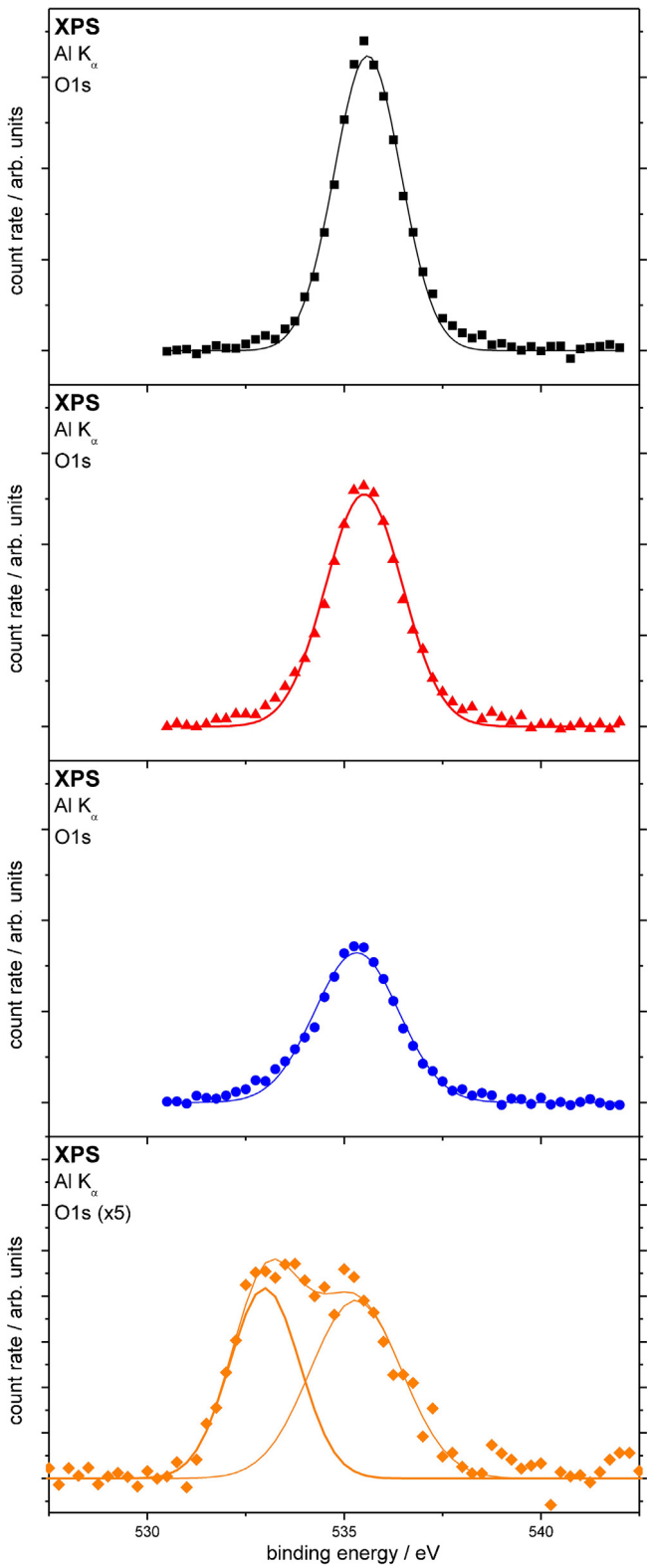

Fig. 3. XPS spectra of the O 1s region of (in order of appearance from top to bottom) a thick film of glucose on Au(1 1 1) as prepared (black lines and squares), after silver adsorption (red lines and triangles) and after subsequent exposure to 3.8×10^{13} L of air (blue lines and circles), as well as a thin film of glucose on Au(1 0 0) after silver adsorption (orange lines and diamonds).

Table 1
Summarized XPS results for the C 1s region.

	Energy	FWHM	Species	Relative intensity
Thick glucose/Au(1 1 1)	286.8	1.47	Mount	0.08
	288.3	1.47	C—C, C—H	0.17
	289.8	1.47	C—O	0.50
	291.2	1.47	O—C—O, C=O	0.18
	292.6	1.47	Mount	0.06
Ag/thick	286.6	1.64	Mount	0.06
glucose/Au(1 1 1)	288.4	1.64	C—C, C—H	0.36
	289.9	1.64	C—O	0.35
	291.3	1.64	O—C—O, C=O	0.16
	292.6	1.64	Mount	0.07
Air/Ag/thick	286.7	1.62	Mount	0.06
glucose/Au(1 1 1)	288.2	1.62	C—C, C—H	0.42
	289.7	1.62	C—O	0.30
	291.1	1.62	O—C—O, C=O	0.15
	292.5	1.62	Mount	0.08
Ag/thin	287.4	1.80		0.29
glucose/Au(1 0 0)	288.0	1.80	C—C, C—H	0.16
	289.5	1.80	C—O	0.36
	290.9	1.80	O—C—O, C=O	0.19

Table 2
Summarized XPS results for the O 1s region.

	Energy	FWHM	Relative Intensity
Thick glucose/Au(1 1 1)	535.6	1.99	1.00
Ag/thick glucose/Au(1 1 1)	535.5	2.3	1.00
Air/Ag/thick glucose/Au(1 1 1)	535.3	2.53	1.00
Ag/thin glucose/Au(1 0 0)	533.0	2.09	0.45
	535.3	2.74	0.55

Table 3
Summarized XPS results for the Ag 3d region.

	Energy	FWHM	Species	Relative intensity
Ag/thick	371.2	1.60	5/2	0.58
glucose/Au(1 1 1)	377.1	1.60	3/2	0.42
Air/Ag/thick	371.1	1.54	5/2	0.58
glucose/Au(1 1 1)	377.1	1.54	3/2	0.42
Ag/thin	370.8	1.29	5/2	0.49
glucose/Au(1 0 0)	372.2	1.29	5/2	0.08
	376.8	1.29	3/2	0.37
	378.3	1.29	3/2	0.06

gets decreased continuously by the silver adsorption as well as the subsequent water dosage. Thereagainst, the silver coated thin film of glucose yields two peaks for the O 1s that might indicate the formation of Ag_2O (cf. [67,68]). All XPS fit results for the O 1s regions have been summarized in detail in Table 2.

Fig. 4 exhibits XPS spectra of the Ag 3d region of a thick film of glucose on Au(1 1 1) as prepared (black lines and squares; top spectrum), after silver adsorption (red lines and triangles; upper middle spectrum) and after subsequent exposure to 3.8×10^{13} L of air (blue lines and circles; lower middle spectrum), as well as a thin film of glucose on Au(1 0 0) after silver adsorption (orange lines and diamonds; bottom spectrum). The thick film of glucose yields the expected peak doublet of Ag $3d_{5/2}$ and Ag $3d_{3/2}$ showing just peak for each one. Even though the background subtraction using the combination of a Shirley-type and a linear background is somehow insufficient, the features shape corresponds very well to a pure film of metallic silver [66]. In contrast to that, the Ag 3d structure of the thin film of glucose after silver adsorption clearly shows a second feature in the shoulders of the peak doublet. This surplus feature may well correspond to Ag_2O [67,68]. All XPS fit results for the Ag 3d regions have been summarized in detail in Table 3.

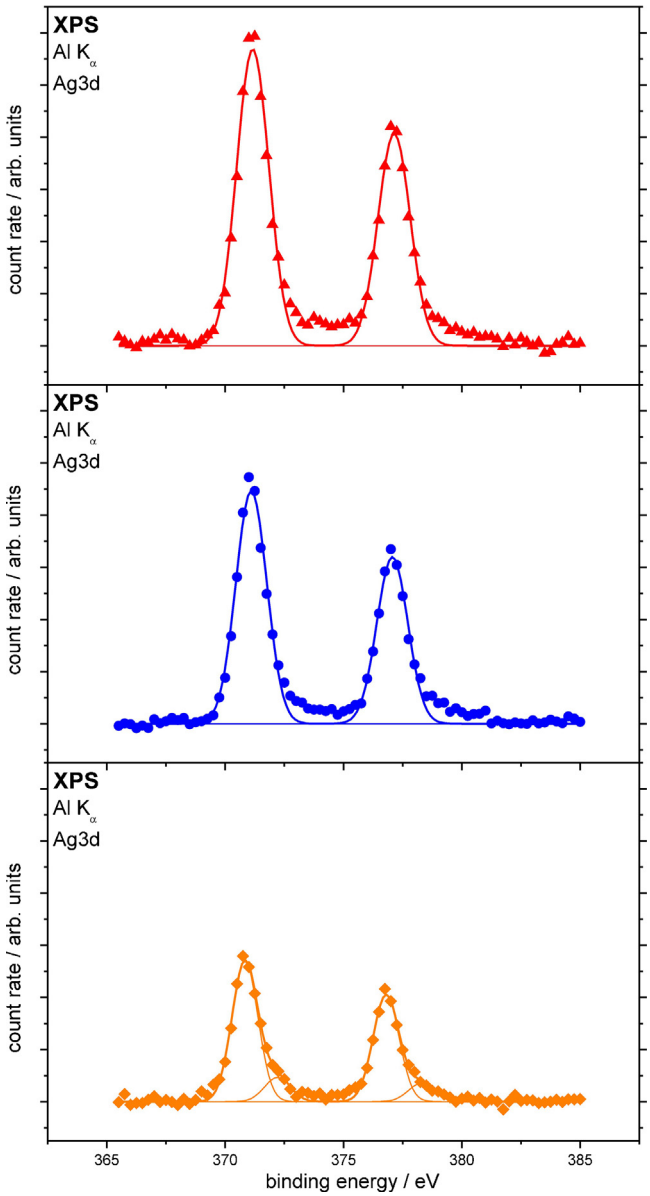

Fig. 4. XPS spectra of the Ag 3d region of (in order of appearance from top to bottom) a thick film of glucose on Au(1 1 1) after silver adsorption (red lines and triangles) and after subsequent exposure to 3.8×10^{13} L of air (blue lines and circles), as well as a thin film of glucose on Au(1 0 0) after silver adsorption (orange lines and diamonds).

3.2. Microscopic results

Fig. 5 shows the topography of the used Au(1 1 1) substrate with a field of view of 1 × 1 μm and a height range of approximately 8.5 nm, one can say the base is rather smooth.

Fig. 6 depicts the thin film of glucose on Au(1 1 1) with adsorbed silver in a range of 5 μm times 5 μm and a height range of circa 350 nm. One can see a closed droplet structure with nanoparticles on top. The nanoparticles have a diameter of about 400 nm and a height of about 50 nm, whereas the droplets have a size of some micrometers. The spacing between the nanoparticles varies between closed and some hundred nanometers.

Fig. 7 displays the thick glucose film on Au(1 1 1) with adsorbed silver in a range of 0.5 μm times 0.4 μm and a height range of 10 nm. It maps, as in Fig. 6 nearby nanoparticles, but with a diameter of about 15 nm and a height of 6 nm

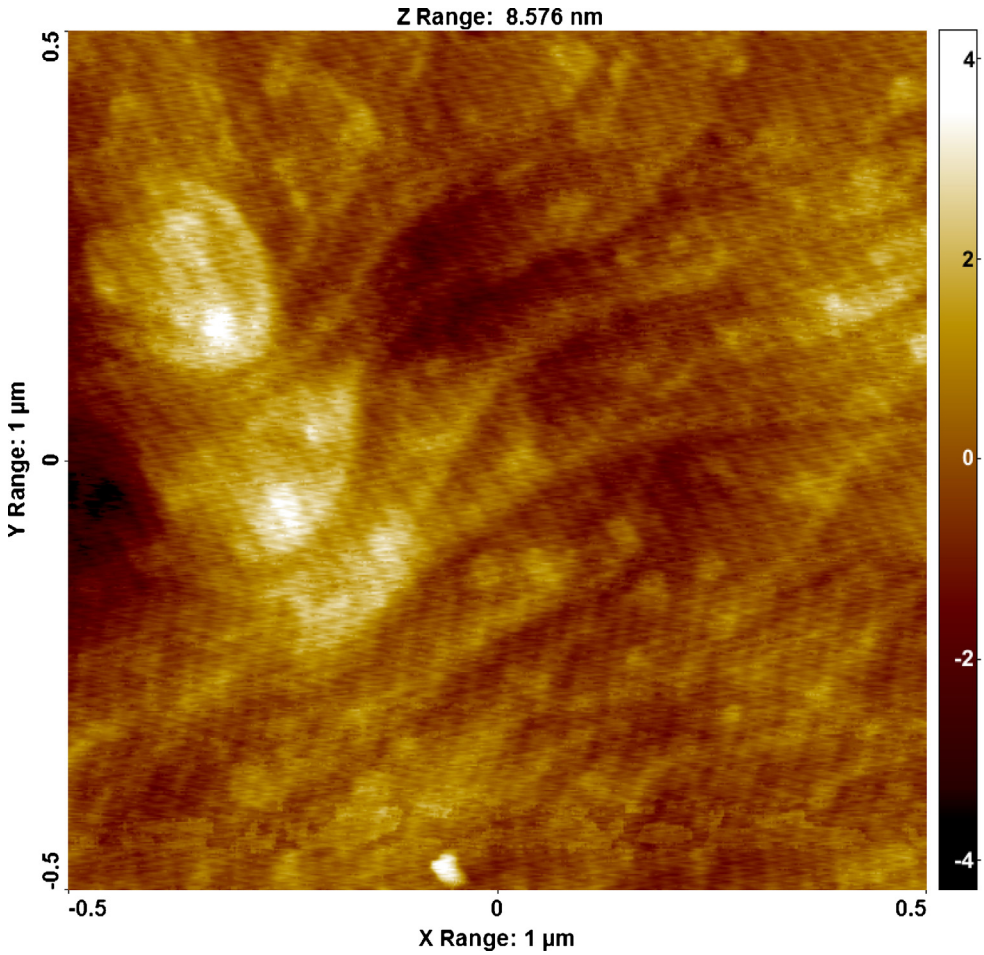

Fig. 5. AFM images of a cleaned Au(1 1 1) substrate (a) and a thick film of glucose on Au(1 1 1) after silver adsorption (b).

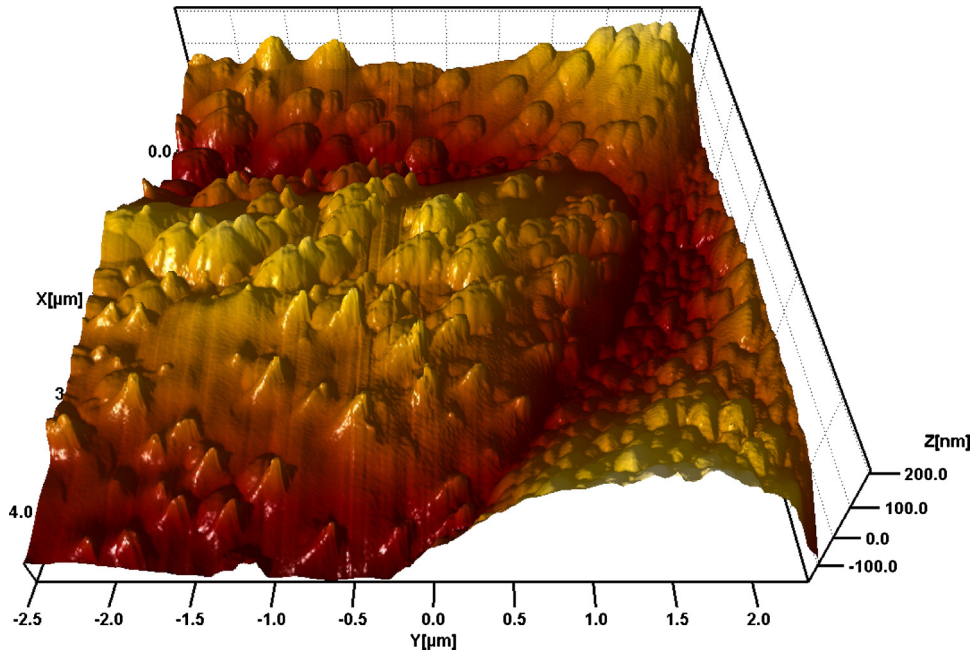

Fig. 6. AFM images of a thin film of glucose on Au(1 0 0) after silver adsorption.

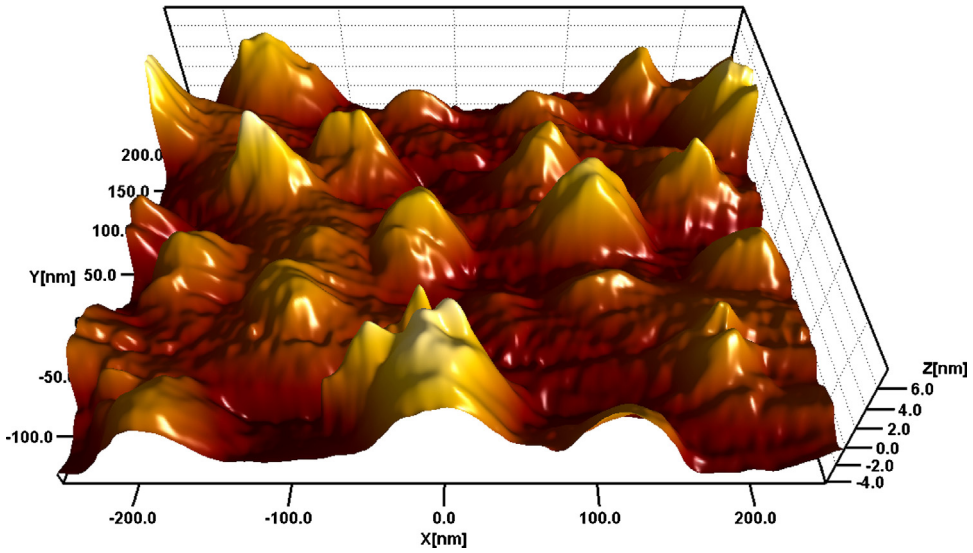

Fig. 7. AFM image of a thin film of glucose on Au(1 0 0) after silver adsorption.

3.3. Discussion

The large droplet structures found in the AFM images are most certainly related to glucose, since the amount of silver evaporated onto the system would not be sufficient at all. The estimation of the film thickness from XPS bases on the assumption of a closed, homogeneous film. Therefore, the film thicknesses estimation for these droplets of glucose will possibly seriously vary from the real amount of glucose adsorbed on the substrate. Nevertheless, these results still give an impression of the order of magnitude and can be well considered to observe changes in the amount of glucose remaining on the surface during the ongoing experiments. Since no relevant changes in the estimated film thicknesses have been found, the desorption or decomposition of glucose can be mostly excluded.

The silver evaporated onto the glucose films did not give any trace in any MIES spectrum, thus it has to be beneath the glucose. For the thin film of glucose, silver structures have been found in UPS, while still no features from the gold substrate could be observed. This indicates that the silver can not be present at the interface between the glucose film and the gold substrate, but has to be within the glucose film.

The smaller particle structures on top of the glucose droplets can't be just due to the adsorbed silver, since no silver was visible in MIES and for the thick film of glucose even no silver was found in UPS. On the other hand, the minimization of surface energies would most probably lead to glucose droplets with homogeneous surfaces, rather than the segregation of smaller structures on top of them. Therefore, the particles also can't be just due to the glucose, but have to result from some kind of interaction between glucose and silver.

Glucose has been found to stabilize Ag nanoparticle in aqueous solutions by Serra et al. [32]. Similar to previous findings on Au nanoparticles [69], the interaction of Ag—O_2 and Ag—OH groups with the OH groups within the glucose via hydrogen bonding has been identified as origin of the stabilizing effect. The same interaction has been found between other metallic nanostructures and glucose, e.g. for Pt nanocrystals that form nanowire-like structures due to stabilization and self-assembly on the interaction with glucose [70].

These interaction between the glucose and the adsorbed silver is considered as the origin for the small particle structures on top of the glucose droplets. The interaction may most probably lead to the encapsulation of silver clusters or particles, once the adsorbed silver atoms would start to agglomerate. On the other hand, the amount of silver would not be sufficient for the found density and size of the particles. Therefore, the glucose film encapsulating the silver nanoparticles has to be considered relatively large, potentially containing silver particles at a diameter of 82 nm for the thick film of glucose and 9.2 nm for the thin film, respectively.

The XPS spectra yield the reduction of OH groups that are attached to the ring after silver adsorption. The water dosage seemed to induce furthermore reduction of the glucose, while no complete decomposition has taken place. This must occur within the glucose film, since MIES and UPS don't show this reduction effect. The reduction of glucose was quite unexpected, since all previous studies only reported the oxidation of glucose toward glucose oxidase [7,25–31,38]. One possible explanation of this reduction effect may be the influence of the spectroscopic investigations. The measuring techniques MIES, UPS and XPS are all based on the emission of electrons, which may lead to a charging of insulated samples. In the case of the silver nanoparticles encapsulated by the glucose, the charging amounted to about 3 V. Even though the reducing behavior has not been investigated electrochemically before, this voltage should probably be enough for the reduction of glucose.

4. Summary

Glucose has been found to adsorb on gold substrates in the form of micro droplets. Due the lack of any reference data on glucose, the valence band structures have been discussed using several model systems which posses all chemical groups of the glucose. The adsorption of silver on glucose has been found to form silver nanoparticles that are encapsulated by a large film of glucose. The origin of this effect has been discussed and a H-bonding between the silver and the glucose has been proposed, according to similar findings from the literature. Furthermore, the silver nanoparticles have been found to reduce glucose, most probably due to the impact of electron spectroscopic measurements.

Acknowledgements

We thankfully acknowledge the provision of the Atomic Force Microscope by the group of Prof. W. Daum (Institut für Energieforschung und Physikalische Technologien, TU Clausthal) as well as the technical assistance of Lienhard Wegewitz and

Dana Schulte Genannt Berthold. Finally, we thank the Deutsche Forschungsgemeinschaft (DFG) for financial support under project numbers MA 1893/18-1 and VI 359/9-1.

References

[1] K.Y. Yang, K.C. Choi, C.W. Ahn, Opt. Express 17 (2009) 11495.
[2] S. Kato, Y. Hirano, M. Iwata, T. Sano, K. Takeuchi, S. Matsuzawa, Appl. Catal. B: Environ. 57 (2005) 109.
[3] H.-Y. Chuang, D.-H. Chen, Nanotechnology 20 (2009) 105704.
[4] C.-N. Lok, C.-M. Ho, R. Chen, Q.-Y. He, W.-Y. Yu, H. Sun, P.K.-H. Tam, J.-F. Chiu, C.-M. Che, J. Proteome Res. 5 (2006) 916.
[5] V. Ilic, Z. Saponjic, V. Vodnic, S. Lazovic, S. Dimitrijevic, P. Jovancic, J.M. Nedeljkovic, M. Radetic, Ind. Eng. Chem. Res. 49 (2010) 7287–7293.
[6] R.M. El-Shishtawy, A.M. Asiri, N.A.M. Abdelwahed, M.M. Al-Obtaibi, Cellulose 18 (2011) 75–82.
[7] C.-H. Xue, J. Chen, W. Yin, S.-T. Jia, J.-Z. Ma, Appl. Surf. Sci. 256 (2012) 2468–2472.
[8] P. Rehn, W. Viöl, Holz Roh. Werkst. 61 (2003) 145–150.
[9] P. Rehn, A. Wolkenhauer, M. Bente, S. Förster, W. Viöl, Surf. Coat. Technol. 174-175 (2003) 515–518.
[10] M. Bente, G. Avramidis, S. Förster, E.G. Rohwer, W. Viöl, Holz Roh. Werkst. 62 (2004) 157–163.
[11] A. Wolkenhauer, A. Meiners, P. Rehn, G. Avramidis, M. Leck, W. Viöl, Holztechnologie 46 (2005) 40–47.
[12] M. Kopp, E. Roddewig, H. Günther, G. Ohms, M. Leck, W. Viöl, Laser Phys. Lett. 2 (2005) 16–20.
[13] A. Wolkenhauer, G. Avramidis, E. Hauswald, H. Militz, W. Viöl, Int. J. Adhes. Adhes. 29 (2009) 18–22.
[14] L. Podgorski, B. Chevet, L. Onic, A. Merlin, Int. J. Adhes. Adhes. 20 (2000) 103–111.
[15] I. Topala, N. Dumitrascu, J. Adhes. Sci. Technol. 21 (2007) 1089–1096.
[16] M. Odraskova, J. Rahel, A. Zahoranova, R. Tino, M. Cernak, Plasma Chem. Plasma Proc. 28 (2008) 203–211.
[17] G. Toriz, M.G. Gutierrez, V. Gonzalez-Alvarez, A. Wendel, P. Gatenholm, A.D. Martinez-Gomez, J. Adhes. Sci. Technol. 22 (2008) 2059–2078.
[18] M. Asandulesa, I. Topala, N. Dumitrascu, Holzforschung 64 (2010) 223–227.
[19] Y. Liu, Y. Tao, X. Lv, Y. Zhang, M. Di, Appl. Surf. Sci. 257 (2010) 1112–1118.
[20] F. Busnel, V. Blanchard, J. Prégent, L. Stafford, B. Riedl, P. Blanchet, A. Sarkissian, J. Adhes. Sci. Technol. 24 (2010) 1401–1413.
[21] M. Gindrat, H.-M. Höhle, K. von Niessen, Ph. Guittienne, D. Grange, Ch. Hollenstein, J. Therm. Spray Technol. 20 (2011) 882–887.
[22] G. Avramidis, A. Wolkenhauer, B. Zhen, H. Militz, W. Viöl, ECWM (2009).
[23] L. Klarhöfer, W. Viöl, W. Maus-Friedrichs, Holzforschung 64 (2010) 331–336.
[24] L. Klarhöfer, PhD thesis, Clausthal Technical University, ISBN 978-3-940394-74-3 (2009).
[25] M. Singh, I. Sinha, R.K. Mandal, Mater. Lett. 63 (2009) 425–427.
[26] W. Shao, Q. Zhao, Surf. Coat. Technol. 204 (2010) 1288–1294.
[27] H. Peng, A. Yang, J. Xiong, Carbohydr. Polym. 91 (2013) 348–355.
[28] L. Csóka, D.K. Bozanic, V. Nagy, S. Dimitrijevic-Brankovic, A.S. Luyt, G. Grozdils, V. Djokovic, Carbohydr. Polym. 90 (2012) 1139–1146.
[29] R. Janardhanan, M. Karuppaiah, N. Hebalkar, T.N. Rao, Polyhedron 28 (2009) 2522–2530.
[30] E.A. Venediktov, A.R.F. Ganiev, V.A. Padokhin, Dokl. Chem. 442 (2012) 34–36.
[31] J. Pal, M.K. Deb, Indian J. Chem. 51 (2012) 821–824.
[32] A. Serra, E. Filippo, M. Re, M. Palmisano, M. Vittori-Antisari, A. Buccolieri, D. Manno, Nanotechnology 20 (2009) 165501.
[33] T. Wen, F. Qu, N.B. Li, H.Q. Luo, Anal. Chim. Acta 749 (2012) 56–62.
[34] S.H. Zuo, Y.J. Teng, H.H. Yuan, M.B. Lan, Anal. Lett. 41 (2008) 1158–1172.
[35] A.S. Rad, A. Mirabi, E. Binaian, H. Tayebi, Int. J. Electrochem. Sci. 6 (2011) 3671–3683.
[36] X. Yang, J. Bai, Y. Wang, X. Jiang, X. He, Analyst 137 (2012) 4362–4367.
[37] M. Jia, T. Wang, F. Liang, J. Hu, Electroanalysis 24 (2012) 1864–1868.
[38] L. Chen, H. Xie, J. Li, J. Solid State Electrochem. 16 (2012) 3323–3329.
[39] J. Tashkhourian, M.R. Hormozi-Nezhad, J. Khodaveisi, R. Dashti, Sens. Actuators B Chem. 158 (2011) 185–189.
[40] A.S. Rad, M. Ardjmand, M. Jahanshahi, A.-A. Safekordi, Korean J. Chem. Eng. 29 (2012) 1063–1068.
[41] H. Quan, S.-U. Park, J. Park, Electrochim. Acta 55 (2010) 2232–2237.
[42] F.M. Cuevas-Muniz, M. Guerra-Balcazar, J.P. Esquivel, N. Sabate, L.G. Arriaga, J. Ledesma-Garcia, J. Power Sources 216 (2012) 297–303.
[43] J.Y. Chen, C.X. Zhao, M.M. Zhi, K.W. Wang, L.L. Deng, G. Xu, Electrochim. Acta 66 (2012) 133–138.
[44] K. Kimura, S. Katsumata, Y. Achiba, T. Yamazaki, S. Iwata, Handbook of HeI Photoelektron Spectra of Fundamental Organic Molecules, Japan Scientific Societies Press (Tokyo) and Halsted Press, New York, 1981.
[45] K. Endo, Y. Kaneda, M. Aida, D.P. Chong, J. Phys. Chem. Solids 56 (1995) 1131–1140.
[46] R.M. France, R.D. Short, Langmuir 14 (1998) 4827–4835.
[47] M. Ono, E. Morikawa, J. Phys. Chem. B 108 (2004) 1894–1897.
[48] P. Boulanger, C. Magermans, J.J. Verbist, J. Delhalle, D.S. Urch, Macromolecules 24 (1991) 2757–2765.
[49] C. Inoue, Y. Kaneda, M. Aida, K. Endo, Polym. J. 27 (1995) 300–309.
[50] S. Shimada, T. Ida, K. Endo, M. Suhara, E.Z. Kurmaev, D.P. Chong, Polym. J. 32 (2000) 1030–1037.
[51] M. Aida, Y. Kaneda, N. Kobayashi, K. Endo, D.P. Chong, B. Chem. Soc. Jpn. 67 (1994) 2972–2979.
[52] K.K. Okudaira, S. Hasegawa, P.T. Sprunger, E. Morikawa, V. Saile, K. Seki, Y. Harada, N. Ueno, J. Appl. Phys. 83 (1998) 4292–4298.
[53] J.P. Moliton, C. Jussiaux-Devilder, T. Trigaud, R. Lazzaroni, J.L. Bredas, S. Galaup, Y. Kihn, J. Sevely, Philos. Mag. B 79 (1999) 793–815.
[54] W. Maus-Friedrichs, M. Wehrhahn, S. Dieckhoff, V. Kempter, Surf. Sci. 249 (1991) 149–158.
[55] D. Ochs, W. Maus-Friedrichs, M. Brause, J. Günster, V. Kempter, V. Puchin, A. Shluger, L. Kantorovich, Surf. Sci. 365 (1996) 557–571.
[56] D. Ochs, M. Brause, B. Braun, W. Maus-Friedrichs, V. Kempter, Surf. Sci. 397 (1998) 101–107.
[57] S. Krischok, O. Höfft, J. Günster, J. Stultz, D.W. Goodman, V. Kempter, Surf. Sci. 495 (2001) 8–18.
[58] J.H. Scofield, J. Electron Spectrosc. Relat. Phenom. 8 (1976) 129–137.
[59] R.F. Reilman, A. Msezane, S.T. Manson, J. Electron Spectrosc. Relat. Phenom. 8 (1976) 389–394.
[60] C. Powell, A. Jablonski, J. Electron Spectrosc. Relat. Phenom. 178 (2010) 331–346.
[61] C.J. Powell, A. Jablonski, NIST Electron Inelastic-Mean-Free-Path Database – Version 1.2, National Institute of Standards and Technology, Gaithersburg, MD, <http://www.nist.gov/srd/nist71.cfm/> (2010).
[62] Y. Harada, S. Masuda, H. Ozaki, Chem. Rev. 97 (1997) 1897.
[63] H. Morgner, Adv. At. Mol. Opt. Phys. 42 (2000) 387.
[64] G. Ertl, J. Kuppers, Low Energy Electrons and Surface Chemistry, VCH Verlag, Weinheim, 1985.
[65] W. Maus-Friedrichs, A. Gunhold, M. Frerichs, V. Kempter, Surf. Sci. 488 (2001) 239–248.
[66] S. Dahle, M. Marschewski, L. Wegewitz, W. Viöl, W. Maus-Friedrichs, J. Appl. Phys. 111 (2012) 034902.
[67] L.S. Kibis, A.I. Stadnichenko, E.M. Pajetnov, S.V. Koscheev, V.I. Zaykovskii, A.I. Boronin, Appl. Surf. Sci. 257 (2010) 404–413.
[68] T.C. Kaspar, T. Droubay, S.A. Chambers, P.S. Bagus, J. Phys. Chem. C 114 (2010) 21562–21571.
[69] J. Liu, P. Raveendran, G. Qina, Y. Ikushima, Chem. Commun. (2005) 2972–2974.
[70] J. Liu, P. Raveendran, G. Qin, Y. Ikushima, Chem. Commun. (2005) 2972–2974.